Chemical Engineering Journal 149 (2009) 325–333

Contents lists available at ScienceDirect

Chemical Engineering Journal

journal homepage: www.elsevier.com/locate/cej

Numerical prediction of particle number concentration distribution in scrubbing-cooling chamber of entrained-flow coal gasifier

Xuan Wu[a,b,*], Tie Li[a], Jie Cai[a], Zhengbiao Peng[a], Zhulin Yuan[a]

[a] School of Energy & Environment, Southeast University, No. 2 Sipailou, Nanjing 210096, China
[b] School of Energy & Environment, Inner Mongolia University of Science & Technology, Baotou 014010, China

ARTICLE INFO

Article history:
Received 2 April 2008
Received in revised form 5 November 2008
Accepted 14 November 2008

Keywords:
Gasifier
Gas–liquid–solid flow
Number concentration
Grading
Capture efficiency

ABSTRACT

The syngas passing through a pool is scrubbed in scrubbing-cooling chamber of coal-water-slurry (CWS) entrained-flow coal gasifier. A three-dimensional Euler–Lagrange model was used to study the distribution of particles in scrubbing-cooling chamber. The simulation of gas and liquid turbulent flow described by RNG k–ε model and the particle flow is modeled using the deterministic trajectory model. The collisions between particles were taken into account by means of direct simulation Monte Carlo (DSMC) method based on the hard-sphere model. Comparisons of computational results with experimental data were also made. The effects of operating conditions and size grading on the distribution of particle number concentration in the chamber was revealed through simulation and analysis. The results indicate that the axial distribution of particle number concentration becomes wave-shaped in pool of scrubbing-cooling chamber. Big particles are ease to subside and small particles are ease to suspend. With changing the particle size grading, the particle number concentration can be changed obviously.

1. Introduction

From the perspective of energy security and environmental sustainability, highly effective utilizations of fossil fuel in energy industries are demanded. Since coal is one of the most important fossil fuels in the world, coal gasification technology appears to be an inevitable choice for power and chemicals production and has a leading place in Clean Coal Technology (CCT) [1]. Power plants such as the Integrated Coal Gasification Combined Cycle (IGCC) are being developed worldwide to use coal more efficiently and cleanly [2–4]. A number of entrained-flow coal gasifiers have been built, and researches on large-scale and high-efficiency entrained-flow coal gasification technology are carried out in China. In CWS entrained-flow coal gasifiers, coal-water-slurry or pulverized coal is gasified at high temperature and under high pressure. The high-temperature syngas produced in gasification chamber comes into scrubbing-cooling chamber, as shown in Fig. 1. Due to the intense heat and mass transfer in cooling ring and cooling tube of scrubbing-cooling chamber, the temperature of the syngas declines dramatically and the molten slag is solidified [5–7]. Then the syngas together with the solidified slag enters into a pool in scrubbing-cooling chamber and direct contacts with liquid. In this process, the solidified slag can be separated from syngas by contacting with liquid from syngas in pool. More slag is expected to subside in the pool to achieve high gas-solid separation rate for optimization design and practical operation of scrubbing-cooling chamber. So various measures of scrubbing performance, such as the complicated structure of the multiphase flow filed, particle concentration, particle motion tendency, etc., are essential to be quantified as functions of the design and operating parameters.

While the understanding of settlement and suspension properties of particles is especially necessary in enhancing scrubbing efficiency of syngas, and the rules of particle movements are important. However few researches have done on this aspect as we know. Furthermore, practically no published information is available on the CFD simulations of the three-phase systems because of the additional complexities associated with the three-phase systems in CWS entrained-flow gasifiers.

The CFD is viable for describing the fluid dynamic and transport behavior of gad–liquid–solid flow systems. There are three basic approaches commonly employed in the CFD for studies of multiphase flows: the Euler–Euler (E–E) method, the Euler–Lagrange (E–L) method, and the direct numerical simulation (DNS) method [8]. Li and Zhang [9] used a combined CFD–VOF–DPM method to simulate the gas–liquid–solid flow in a fluidized bed, whereas in their study the effect of turbulent flow was not considered. Jin [10] developed a multi-scale model for the gas–liquid–solid three-phase fluidized beds on the basis of the principles of energy-minimization multi-scale (EMMS) method. Murthy [11] treated gas, liquid and solid as different continua, and simulated three-phase stirred

* Corresponding author. Tel.: +86 25 83791273.
E-mail address: wuxuan5110@sina.com (X. Wu).

1385-8947/$ – see front matter © 2008 Elsevier B.V. All rights reserved.
doi:10.1016/j.cej.2008.11.027

Nomenclature

C_d	drag force coefficient
C_k	volume fraction of the kth phase
F	force (N)
G_{ij}	relative velocity between particles (m/s)
l	true number of particles
m	mass of particle (kg)
N	sample number of particles
p	pressure (N/m^2)
p_{ij}	probability of particle–particle collision
r_p	radius of particle (m)
R	random number $0 \le R \le 1$
Re_p	particle Reynolds number
u	velocity (m/s)

Greek letters

α_k	inverse effective turbulent Prandtl number for k
α_ε	inverse effective turbulent Prandtl number for ε
ε	eddy dissipation rate (m^2/s^3)
μ	dynamic viscosity (kg/s)
ρ	averaged density (kg/m^3)
ρ_k	density of the kth phase (kg/m^3)
ω	angular velocity of particles (rad/s)

Superscripts

0	before the collision

Subscripts

c	continuum phase
i,j	spatial coordinate indices
p	particle phase

reactor using Euler–Euler method. Zhang et al. [12] developed an Euler–Lagrange model for gas–liquid–solid flows in three-phase slurry reactors, in which the liquid flow is modeled using a volume-averaged system of governing equations, and motions of bubbles and particles are evaluated by the Lagrange approach. Wang et al. [13] performed a series of simulations of three-phase flow in hydrocyclones with different configurations of vortex finder using the Reynolds Stress Model for gas and liquid phase, the volume of

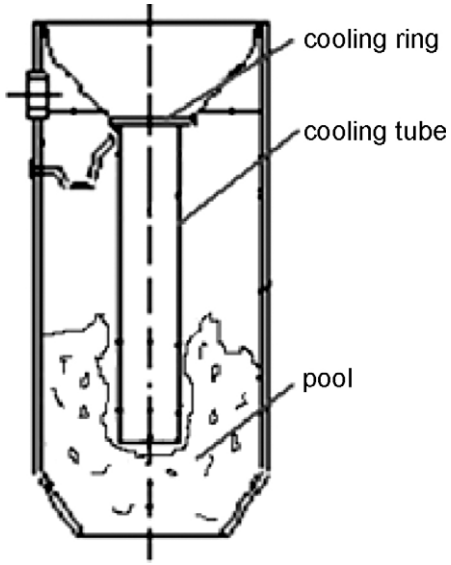

Fig. 1. Schematic diagram of a scrubbing-cooling chamber.

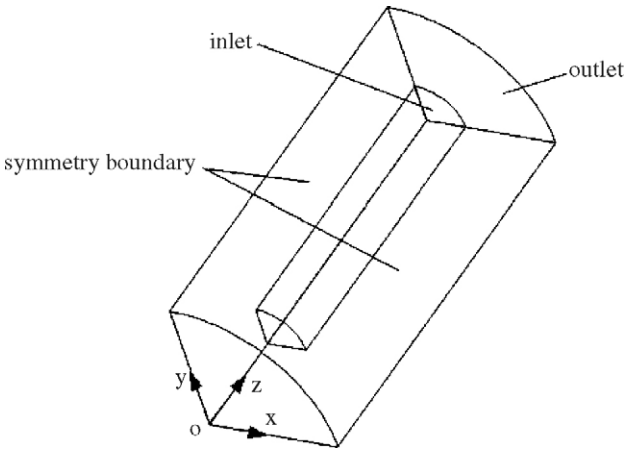

Fig. 2. Three-dimensional computational model of chamber in 90° sector.

fluid multiphase model for the interface between the liquid and air and a stochastic Lagrange method for particle flow.

Our work is focus on numerical simulation investigations on the distribution of particles number concentration in scrubbing-cooling chamber of CWS entrained-flow gasifiers. A three-dimensional Euler–Lagrange model is employed to evaluate the three-phase flows. The model offers a way to examine the effects of different operation parameters, such as different gas velocity, particle size grading, etc., on the particle distribution, particle movement characteristics and particle capture efficiency in scrubbing-cooling chamber. Computational results are compared with experimental data to show the validation of the mathematical model and the computational method.

2. Mathematical models

The symmetrical property is existed in the mechanism of scrubbing-cooling chamber in coal-water-slurry (CWS) entrained-flow gasifiers. Therefore, a 90° radial sector of the scrubbing-cooling chamber with symmetry boundary conditions at both vertical sides is set up in order to improve the computational efficiency. A three-dimensional computational model in 90° sector is modeled with symmetry boundary conditions as shown in Fig. 2. And an axial section of the computational model is shown in Fig. 3.

This study is based on the following assumptions: (i) the particles are spheres. (ii) Heat and mass transfer are ignored in flow process. (iii) The influence of water film on the particles in cooling tube is not considered. In our present work, an Euler–Lagrange method has been adopted to describe the flow behavior of each phase, where the gas and liquid are respectively treated as different continuous phase, the particles are treated as discrete phase. The gas–liquid flow is modeled as turbulent, described by the RNG k–ε model. The interface between the liquid and air core is modeled by the volume of fluid model, and the results are then used in the simulation of particle flow described by the deterministic trajectory model. In present work, a dilute particle concentration is considered. Therefore, one-way coupling between discrete phase and continuous phase is carried out. The key features of these models are briefly described as follows.

2.1. Gas–liquid phase

The continuity equation:

$$\frac{\partial u_i}{\partial x_i} = 0 \tag{1}$$

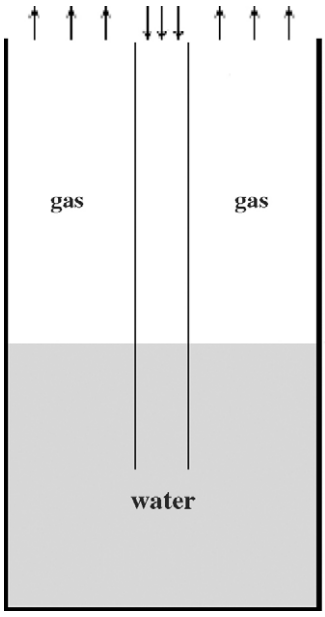

Fig. 3. Schematic diagram of axial section of computational model.

The momentum equation:

$$\frac{\partial u_i}{\partial t} + \frac{\partial}{\partial x_j}(u_i u_j) = -\frac{1}{\rho}\frac{\partial p}{\partial x_i} + \frac{1}{\rho}\frac{\partial}{\partial x_j}\left[\mu\left(\frac{\partial u_i}{\partial x_j} + \frac{\partial u_j}{\partial x_i}\right)\right] + \frac{\partial}{\partial x_j}(-\overline{u_i' u_j'}) + F_v \quad (2)$$

where p is the pressure, $-\rho\overline{u_i' u_j'}$ is Reynolds stress term, the velocity components is decomposed into the mean velocity $\bar{u}_i$ and fluctuating velocity u_i' velocity, i.e.

$$u_i = \bar{u}_i + u_i' \quad (3)$$

The volume of fluid model represents multiphase flow with a fractional volume function C_k, it takes the values $0 \le C_k \le 1$ in the cells:

$C_k = 1$	in cells full of the kth fluid
$C_k = 0$	in cells devoid of the kth fluid
$0 < C_k < 1$	the cells contain the interface between the kth fluid and other fluid

Species mass conservation requires C to fulfil the following equation:

$$\frac{\partial C_k}{\partial t} + u_i \frac{\partial C_k}{\partial x_i} = 0 \quad (4)$$

where u_i is the velocity component in direction i. The properties appearing in Eqs. (1) and (2) are related to the volume fraction of all phases as follows:

$$\rho = \sum C_k \rho_k, \qquad \mu = \frac{\sum C_k \rho_k \mu_k}{\sum C_k \rho_k} \quad (5)$$

In our simulation, surface tension is applied using the continuous surface force (CSF) scheme [14]. The addition of surface tension to the volume of fluid method is modeled by a source term F_v in the momentum equation:

$$F_s = \sigma k \ \nabla C_k \quad (6)$$

where σ is surface tension coefficient. The surface curvature k is defined in terms of the divergence of the unit normal $\hat{n}$:

$$k = \nabla \cdot \hat{n} \quad (7)$$

where surface normal $\hat{n} = n/|n|$.

At the wall, the surface normal n at the live cell next to the wall is define in terms of the contact angle, θ, between the interface and the wall by

$$n = n_w \ \cos\theta_w + t_w \sin\theta_w \quad (8)$$

where n_w and t_w are the unit vectors normal and tangential to the wall, respectively. All the results reported in this study are obtained with the contact angle of 90°.

The present work deals with the unsteady flow, which is modeled as turbulent flow by the RNG k–ε model. The RNG k–ε model is derived using a rigorous statistical technique called renormalization group theory by Yakhot and Orszg [15]. From the examples of different turbulent flow features, especially flows having strong streamline curvature, vortices, rotation, the RNG k–ε model is proved to provide accurate results [16]. Furthermore, the constants used in the RNG k–ε model are evaluated by theory and not by empiricism.

The kinetic energy of turbulence:

$$\rho\frac{\partial k}{\partial t} + \frac{\partial}{\partial x_i}(\rho k u_i) = \frac{\partial}{\partial x_j}\left(\alpha_k \mu_{\text{eff}} \frac{\partial k}{\partial x_j}\right) + G_k - \rho\varepsilon \quad (9)$$

The dissipation rate of kinetic energy of turbulence:

$$\rho\frac{\partial \varepsilon}{\partial t} + \frac{\partial}{\partial x_i}(\rho \varepsilon u_i) = \frac{\partial}{\partial x_j}\left(\alpha_\varepsilon \mu_{\text{eff}} \frac{\partial \varepsilon}{\partial x_j}\right) + C_{1\varepsilon}\frac{\varepsilon}{k}G_k - C_{2\varepsilon}^*\rho\frac{\varepsilon^2}{k} \quad (10)$$

where the quantities α_k, α_ε is inverse effective turbulent Prandtl number for k and ε. The model values for $C_{1\varepsilon}$ is 1.42. G_k is the generation of turbulence kinetic energy due to the mean velocity gradients.

The coefficient $C_{2\varepsilon}^*$ contains the additional source, which is the main difference between the RNG k–ε turbulence models and the standard k–ε turbulence models. It is constant for standard k–ε model but for RNG k–ε, $C_{2\varepsilon}^*$ takes the following form:

$$C_{2\varepsilon}^* = C_{2\varepsilon} + \frac{C_\mu \rho \eta^3 (1 - \eta/\eta_0)}{1 + \beta\eta^3} \quad (11)$$

where $C_{2\varepsilon} = 1.68$, $\eta_0 = 4.38$, $\beta = 0.012$.

2.2. Particle phase

Fully 3D particles flow is modeled by the deterministic trajectory model and collisions between particles are modeled by means of the direct simulation Monte Carlo (DSMC) method [17]. In the DSMC method, physical particles are replaced by sampled particles of a Small Number. As the flow filed is represented by the filed of sampled particles, the computation time can be reduced drastically [18]. The translational motion of a particle in the liquid or gas phase is governed by Newton's second law of motion:

$$m_p \frac{du_p}{dt} = F_d + F_m + F_f + F_g + F_b \quad (12)$$

where m_p and u_p are the mass and velocity of particles respectively. On the right-hand side of Eq. (12), F_d is the drag force, F_m is the Margnus force, F_f is add mass force, F_g is gravity force and F_b is the buoyancy force.

The drag force is given by

$$F_d = \frac{\pi r_p^2}{2} C_d \rho_c |u_c - u_p| (u_c - u_p) \quad (13)$$

Here r_p is the particle radius, ρ_c is density of liquid if particle lie in liquid. Otherwise, ρ_c is gas density when particle lie in gas. C_d is the drag coefficient, which is a function of the particle Reynolds

number Re_p. It can be estimated by the following equations [18]:

$$C_d = \begin{cases} \frac{24}{Re_p}(1 + 0.15\ Re_p^{0.687}) & Re_p < 1000 \\ 0.44 & Re_p \geq 1000 \end{cases} \quad (14)$$

The added mass force accounts for the resistance of the fluid mass that is moving at the same acceleration as the particle:

$$F_f = \frac{2}{3}\pi r_p^3 \rho_c \frac{d}{dt}(u_c - u_p) \quad (15)$$

The Margnus force is given as

$$F_m = \pi r_p^3 \rho_c \omega (u_c - u_p) \quad (16)$$

The probability of particle i collides with other particle during a time step Δt is given by [17]:

$$P_i = \sum_{j=1}^{N} P_{ij} = \sum_{j=1}^{N} 4\frac{l}{N}\pi r_p^2 G_{ij}\ \Delta t \quad (17)$$

where N is the number of sample particles. l is the number of real particles. G_{ij} is the relative velocity between particle i and particle j.

The modified Nanbu method [17] is used to choose the collision partner. Firstly, a random number R is extracted from a generator which has a uniform distribution ranging from zero to unity. A collision partner j is selected according to

$$j = \text{int}[R \times N] + 1, \quad j \neq i \quad (18)$$

where int$[R \times N]$ is defined by the integer part of $R \times N$. And

$$R > \frac{j}{N} - P_{ij} \quad (19)$$

If this relation is satisfied, the particle i could collide with particle j during one time step Δt. The velocity of particles is replaced by the post-collision velocity. The post-collision linear velocity and angular velocity of particle i and j can be determined through the hard-sphere model as follows [17].When $(n \cdot G^0/G_{ct}^0) < (2/7)(1/f(1+e))$,

$$\begin{aligned} V_i &= V_i^0 - (n - ft)(n \cdot G^0)(1+e)\frac{m_j}{m_i + m_j} \\ V_j &= V_j^0 + (n - ft)(n \cdot G^0)(1+e)\frac{m_i}{m_i + m_j} \\ \omega_i &= \omega_i^0 + \frac{5}{d_i}(n \cdot G^0)(n \times t)(1+e)\frac{m_j}{m_i + m_j} \\ \omega_j &= \omega_j^0 + \frac{5}{d_j}(n \cdot G^0)(n \times t)(1+e)\frac{m_i}{m_i + m_j} \end{aligned} \quad (20)$$

When $(n \cdot G^0/G_{ct}^0) \geq (2/7)(1/f(1+e))$

$$\begin{aligned} V_i &= V_i^0 - \left[(1+e)(n \cdot G^0)n + \frac{2}{7}|G_{ct}^0|t\right]\frac{m_j}{m_i + m_j} \\ V_j &= V_j^0 + \left[(1+e)(n \cdot G^0)n + \frac{2}{7}|G_{ct}^0|t\right]\frac{m_i}{m_i + m_j} \\ \omega_i &= \omega_i^0 - \frac{10}{7d_i}|G_{ct}^0|(n \times t)\frac{m_j}{m_i + m_j} \\ \omega_j &= \omega_j^0 - \frac{10}{7d_j}|G_{ct}^0|(n \times t)\frac{m_i}{m_i + m_j} \end{aligned} \quad (21)$$

where f is the friction coefficient of Coulomb's friction law. e is the reversion coefficient. G^0 is the relative velocity of the particle centers before and after collision. t is the unit vector in the tangential direction, given by

$$t = \frac{G_{ct}^0}{|G_{ct}^0|} \quad (22)$$

G_{ct}^0 is the tangential component of the relative velocity of the contact point before collision, and is given by

$$G_{ct}^0 = G^0 - (G^0 \cdot n)n + 0.5 \times d_i\omega_i^0 \times n + 0.5 \times d_j\omega_j^0 \times n \quad (23)$$

where

$$G^0 = V_i^0 - V_j^0 \quad (24)$$

When particles move in liquid, the liquid shear effect between particles becomes important when two particles move close to each other in liquid-solid systems [19,20]. The close–distance interaction (CDI) model is used. The details and justification of CDI model are referred to Refs. [19,20].

3. Numerical solution

The numerical solution of the continuity and momentum equations for gas–liquid continuous phase is obtained using the CFD code FLUENT 6.2, which is a vertex-centered code based on the finite volume numerical method. Unsteady simulations are performed for a gas passing through pool process in scrubbing-cooling chamber. The simulation of gas–liquid two phases has been carried out using Euler–Euler model. The finite volume method is employed to solve a set of governing equations. All terms of the governing equations are discredited using the second-order upwind scheme. The pressure–velocity coupling is obtained using the SIMPLE algorithm. The convergence criterion is set at 10^{-3} for all the equations. All walls are treated as non-slip boundaries with standard wall function. A "velocity-inlet" boundary condition is used at the inlet, and the outlet uses the "pressure-outlet" boundary condition. The inlet gas velocity and particle velocity are same value.

The simulation of particle phase is performed in Lagrange frame using self-written program in VC++ language. Trajectory tracking of each particle is performed in every time step. The time step for numerical integration is taken sufficiently small compared with the mean free time of the particles. The particle flow field is divided into small cells in which a sufficient number of sampled particles exist. These cells can be used for particle flow calculations do not necessarily coincide with the cells for fluid calculations. According to the volume fraction of gas and liquid, whether particle lies in gas or liquid is decided. When the gas phase fills the whole mesh, the forces acting on the particles from gas are considered. Otherwise, when a mesh is full of liquid phase, the forces acting on the particles from liquid are considered. When gas and liquid hold the mesh together, we decide whether particles lie in gas or liquid according to the volume fraction of gas and liquid. In this study, we assume that the particles will be captured by liquid once they come into liquid phase.

In order to check the sensitivity of the simulation result on the grid size, three grid spacing: 1 cm, 0.5 cm and 0.1 cm are selected. Comparison of the three cases showed that the latter two cases did not generate a noticeable difference in simulation results. The distribution grid may be considered to provide acceptable, grid independent solutions. Therefore, a grid spacing of 0.5 cm is used throughout the rest of the calculations in this paper.

4. Results and discussion

4.1. Model verification

It is necessary to verify the model before its application for numerical experiment. To verify the accuracy of the computational scheme, the model predictions are compared with the experimental data of He [21]. The schematic diagram of the scrubbing-cooling chamber experimental system is given in Fig. 4.

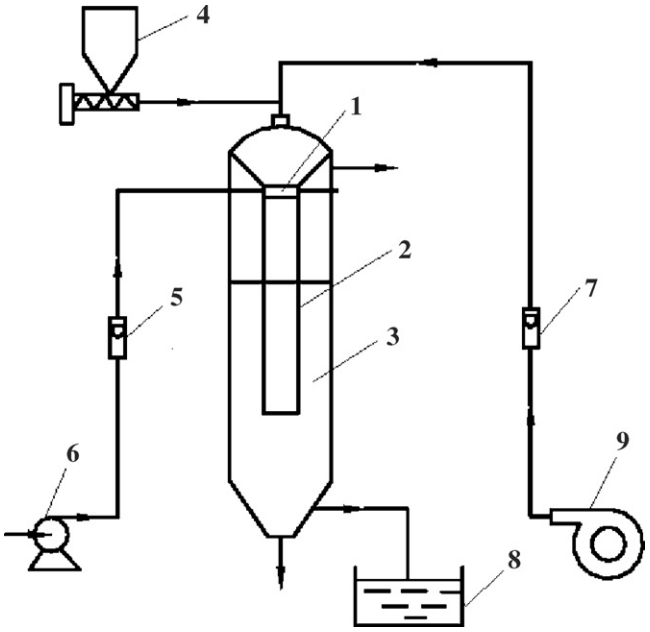

Fig. 4. Schematic diagram scrubbing-cooling chamber of CWS entrained-flow gasifier experimental system. 1-cooling ring, 2-cooling tube, 3-pool, 4-worm feeder, 5-liquid flow meter, 6-water pump, 7-gas flow meter, 8-cistern, 9-roots blower.

The mass fraction of particles along the height of scrubbing-cooling chamber is measured via experiment, in which the feeding rate of cinders particles is 18 kg/h, and the gas flux is 300 m^3/h. The distribution of feeding particle diameter is shown in Fig. 5 and the comparison of simulated axial mass fraction of particles with experimental results is shown in Fig. 6. In the experiment, the feeding rate of coal particles is 18 kg/h, i.e. about 40,000 particles per second. It is well known that the Lagrange method is tracking the movement of each particle. Unfortunately, the present computer hardware conditions are very limited for the large amount of particles according to the experiment. Therefore, the numerical feeding rate is smaller than in the experimental counterpart in order to improve the computational efficiency. Even though the initial size distribution of the feeding particles are adjusted to be equivalent with that in experiment, inaccuracy cannot be avoided due to the differences of entered quantity of particles and time of obtaining data. But in comparison with experimental results, the model predictions are qualitatively consistent with the experimental result. The established models are proved to be reasonable, based on these models the following numerical simulations about the distribution of particle number concentration are carried out.

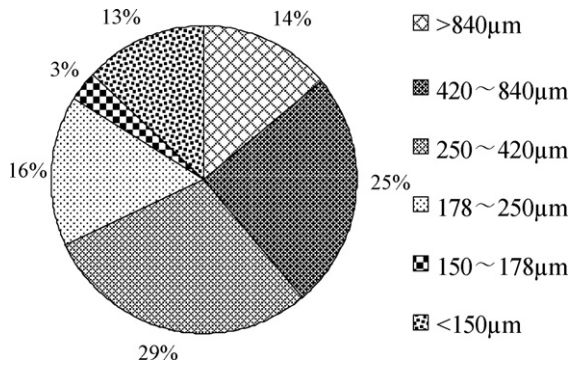

Fig. 5. The distribution of feeding particle diameter in experiment.

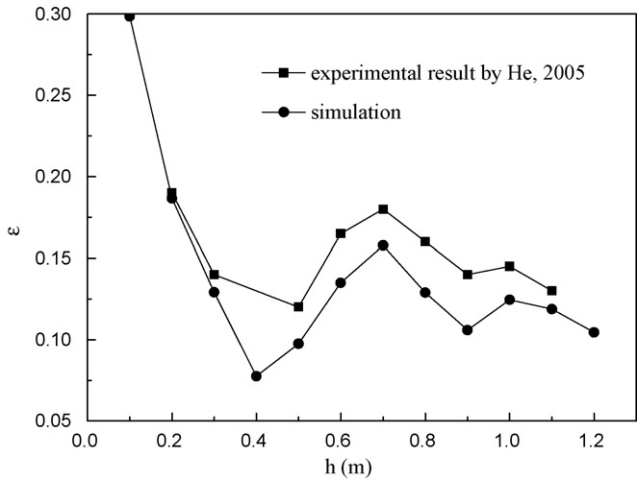

Fig. 6. Comparison of simulated axial mass fraction of particles with experimental results.

Table 1
The calculation parameters used in numerical calculation.

Parameter	Value	Parameter	Value
Gas density (kg m^{-3})	1.29	Liquid density (kg m^{-3})	1000
Gas viscosity (m^2 s^{-1})	2.38×10^{-5}	Liquid viscosity (m^2 s^{-1})	1.00×10^{-6}
Gas velocity (m s^{-1})	1, 3, 5	Particle density (kg m^{-3})	2540
Particle friction coefficient	0.3	Time step (s)	0.0001
Particle reversion coefficient	0.8	Particle diameter (mm)	0.01, 0.05, 0.3, 1, 10

4.2. Gas–liquid flow studies

The flow conditions and parameters used in the simulation are summarized in Table 1. In scrubbing-cooling chamber of coal-water-slurry gasifier, the process of syngas passing through the pool is a typical process of top-submerged gas injection. Top-submerged gas injection is less commonly used than bottom or side gas injection, which indicates the small amount of numerical simulation work on the problem in the literature. No attempt was made to simulate free surface distortions and splashing induced by the gas injection [22].

Fig. 7 shows movie frames of the fluid in scrubbing-cooling chamber at selected times after gas injection is started with an average gas inlet velocity of 1.0 m/s, denoting the volume fraction distribution of the gas phase. When gas injects into water, direction of gas flow breaks rapidly. The splash droplets are thrown above the quiescent free surface height all over the chamber, although the highest ejections occur close to the cooling tube. Bubble rise and liquid ejections in the chamber are chaotic, with no bubbles and splash drops consistently following any single well-defined trajectory over time.

Fig. 8 shows the pressure signal at the top of the inside of the lance. The pressure signal is clearly periodic change. The Fast Fourier Transform (FFT) of the pressure signal shows the constant bubbling frequency of 4 Hz. These conclusions of this study are in agreement with the physical experiment [23].

4.3. Particle number concentration studies

Table 2 summarizes the particle size grading for four different cases studied. The following simulations are performed based on grading 1. Fig. 9 shows the spatial distribution of particles with dif-

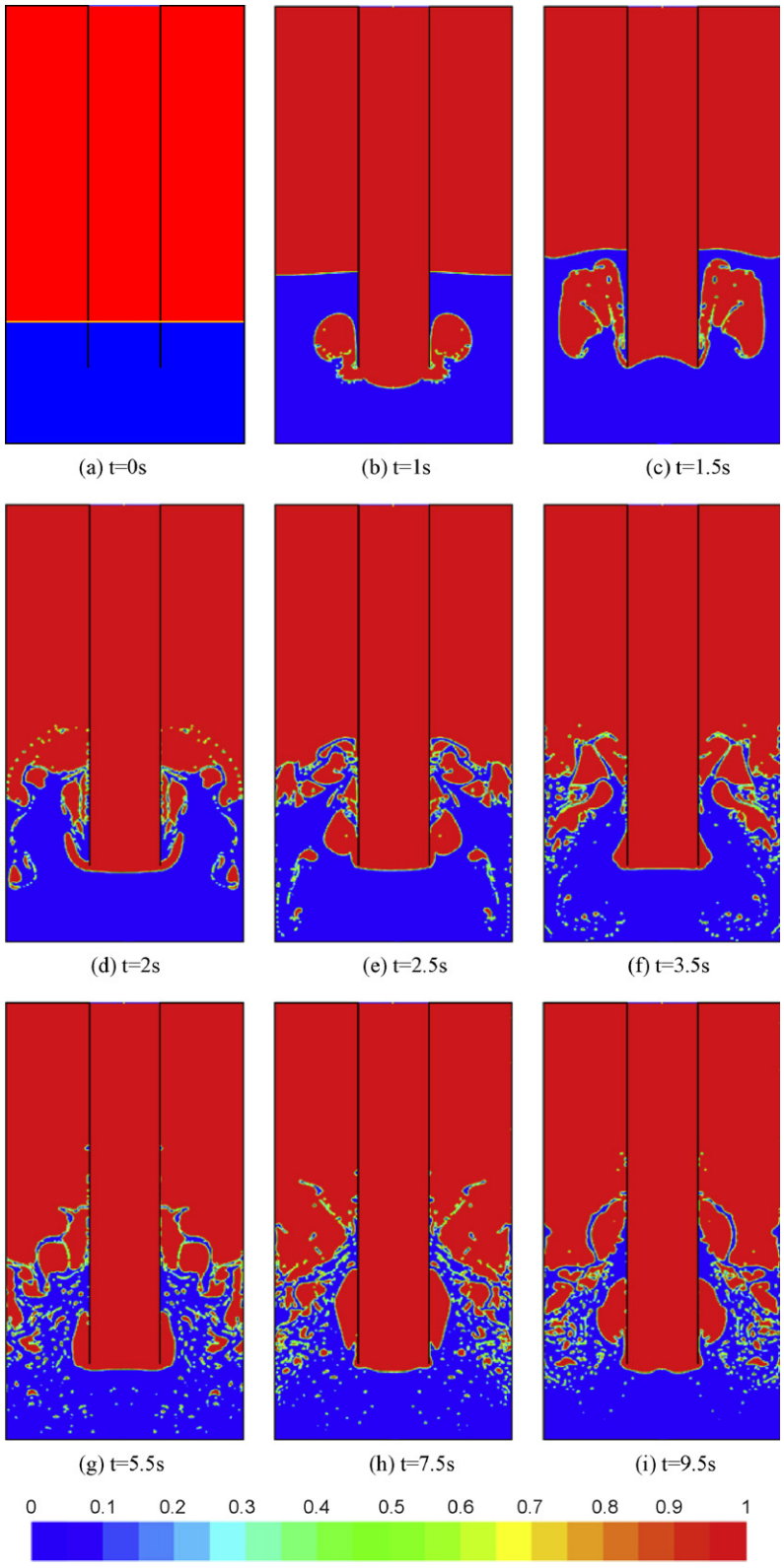

Fig. 7. The distribution of liquid and gas at selected times for the injection of gas into water at 1.0 m/s.

ferent sizes in scrubbing-cooling chamber at an average gas inlet velocity of 3.0 m/s. Fig. 9 represents the snapshots of the movement of particles of different sizes. Particles of five different diameters are chosen to track their trajectories and distributions in chamber, where red, blue, green, black and orange represent 0.01, 0.05, 0.3, 1 and 10 mm particles, respectively. The big particles (black and orange) accumulate at the bottom of the pool in scrubbing-cooling chamber. The small particles (green and blue) concentrate around the outlet of cooling tube and the liquid surface. And some of fine particles (red) escape from the pool along the upwards flow.

The axial distribution of particles number concentration at different gas inlet velocities is shown in Fig. 10. The axial distribution of

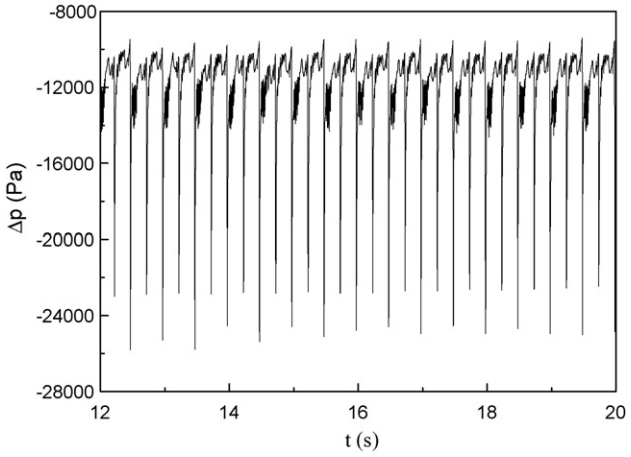

Fig. 8. The characteristics of pressure fluctuation for the injection of air into water at 1.0 m/s.

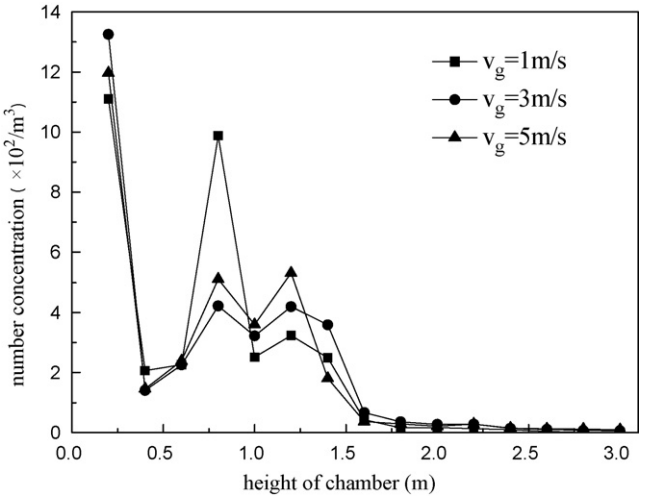

Fig. 10. Axial distribution of particle number concentration.

Table 2
The particle size grading used in numerical calculation.

Particle diameter (mm)	Grading 1	Grading 2	Grading 3	Grading 4
0.01	0.2	0.3	0.15	0.35
0.05	0.2	0.3	0.15	0.1
0.3	0.2	0.2	0.20	0.1
1	0.2	0.1	0.25	0.1
10	0.2	0.1	0.25	0.35

particles number concentration becomes wave-shaped with three peak values. The big particles are easy to separate from gas and accumulated at the bottom of the pool in scrubbing-cooling chamber under gravity. Therefore, the maximal value of particle number concentration appears at the bottom of the pool. At the outlet of cooling tube, particles come into pool and diffuse in the liquid. Therefore, the particle number concentration achieves another peak value. The small particles are not easy to subside, so they suspend in the region of liquid surface. Therefore, the particle number concentration rises again in the region of liquid surface. The suspended particles in the region of liquid surface may be entrained with entrained liquid by the flowing gas. The fine particles escape from the pool along the upwards flow. The particle number concentration decreases along the height of chamber below height with 0.4 m. At the height of 0.4 m–0.7 m, the particle number concentration increases with chamber height increases. The height of cooling pipe outlet is 0.7 m. And particles come into the pool at this height, thus another peak value of particle number concentration is achieved. The height of liquid surface locates in 0.7–1.2 m. The captured small particles suspend near the liquid surface and the particle number concentration rises again. Over the height of 1.2 m, the particle number concentration decreases linearly with height of scrubbing-cooling chamber. On the whole, with the increase of chamber height, the particle number concentration decreases gradually.

As shown in Fig. 10, the number concentration of diffused or suspended particles increases with the gas velocity increases. When the velocity of gas inlet is 1 m/s, some of small particles concentrate around the outlet of cooling tube due to the decrease of the effects of gas and liquid on particles.

In order to reveal the changes of particle capture efficiency with time, the capture efficiency, η, is defined as

$$\eta = \frac{n(t)}{N(t)} \times 100\% \tag{25}$$

where $n(t)$ and $N(t)$ are the quantity of particles captured by liquid and entered particles with gas during the period from initial time t_0 to t time, respectively.

Fig. 11 shows the change process of particle capture efficiency dependence of time at different gas inlet velocity. It quantitatively gives the separation properties of gas–solid phase. The capture efficiency of particles gradually increases to reach a steady value as the time increases. The total change process of particle capture efficiency comprises the quick increase stage and the gradual steady stage. The capture efficiency increases with increasing gas inlet velocity. The steady values of capture efficiency are 91.1%, 96.7%

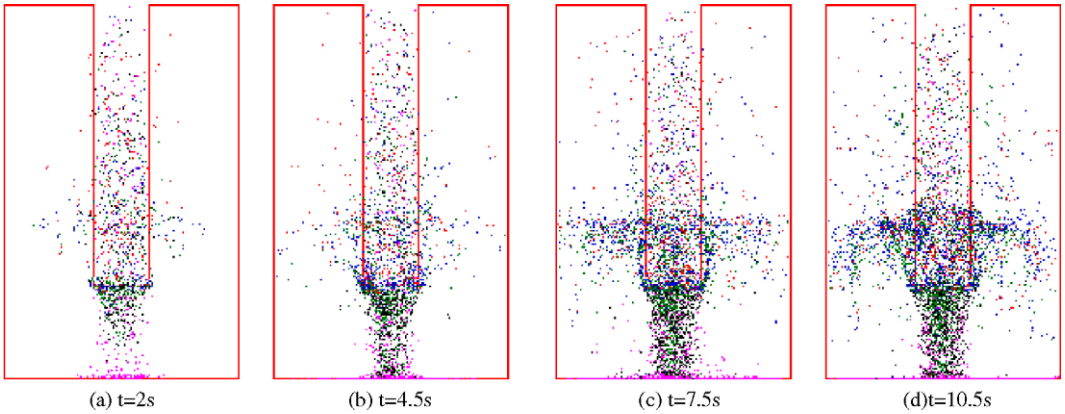

Fig. 9. Particle size distribution in scrubbing-cooling chamber at different time.

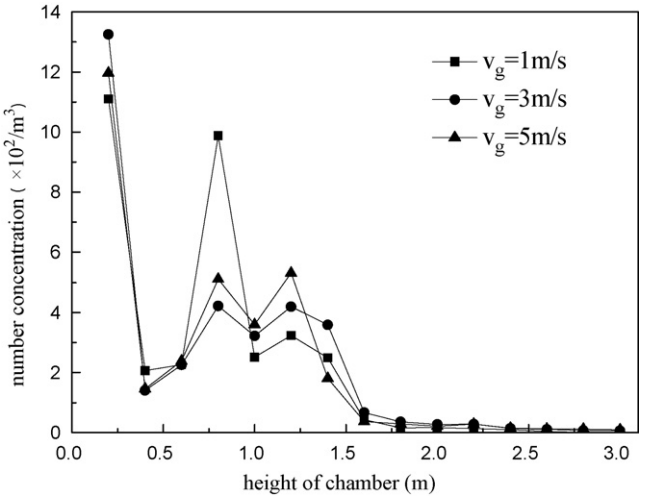

Fig. 11. Capture efficiency of particles dependence of time at different gas velocity.

and 98.1% with gas inlet velocity of 1 m/s, 3 m/s and 5 m/s, respectively. However, the effect of gas velocity on the capture efficiency reduces gradually as the gas velocity increases.

Fig. 12 shows the capture efficiency of particles with different sizes dependence of time. The capture efficiency increases with the increase of particle size. For particles with a certain diameter, the capture efficiency gradually increases to reach a steady value as the time increases. The steady value of capture efficiency is 98.1%, when particle diameter is 50 μm, and the capture efficiency is 97% and 88.2% with particle diameter of 20 μm and 10 μm, respectively. The capture efficiency increases with increasing particle diameter. But the effect of gas velocity on the particles capture efficiency gradually reduces as the particle diameter increases. The simulation results are in agreement with the conclusion drawn by the scrubbing-cooling chamber practical operation.

The axial distribution of number concentration of particles with different diameter is shown in Fig. 13. Due to the forces acting on particles varies with the particles different diameter, the axial distribution of different diameter particles is difference. The big particles subside to the bottom of the pool rapidly, so they have higher number concentration at the bottom of the pool. It is obvious that the bigger size particles, the higher the separation rate gets. Due to the better flow with gas, the axial distribution of particles with 0.01 m diameter is smooth. And the other size particles concentrate around the outlet of cooling tube or the liquid surface.

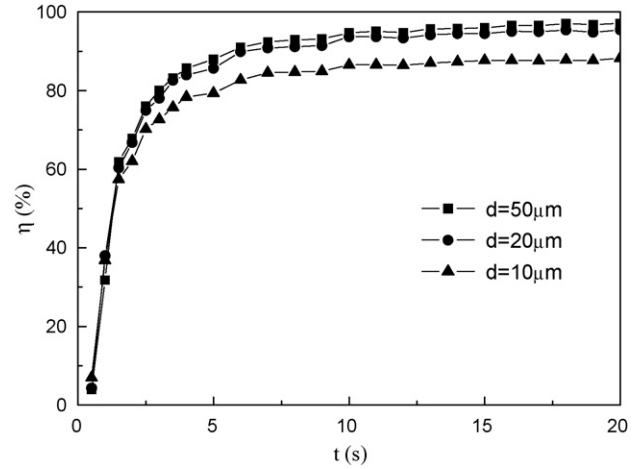

Fig. 12. Capture efficiency of particles with different diameter dependence of time.

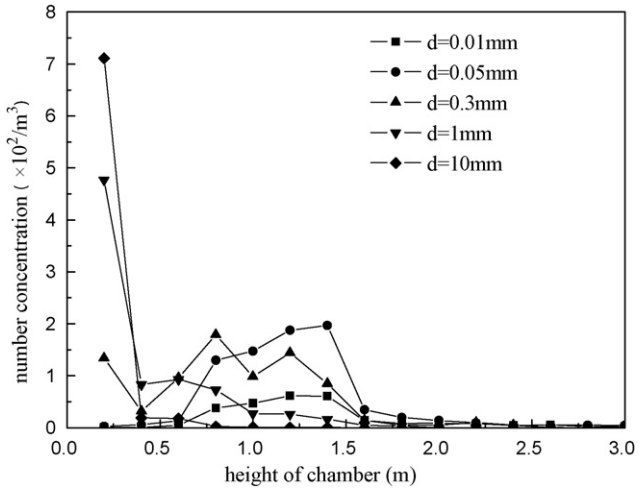

Fig. 13. Axial distribution of number concentration of particles with different diameter.

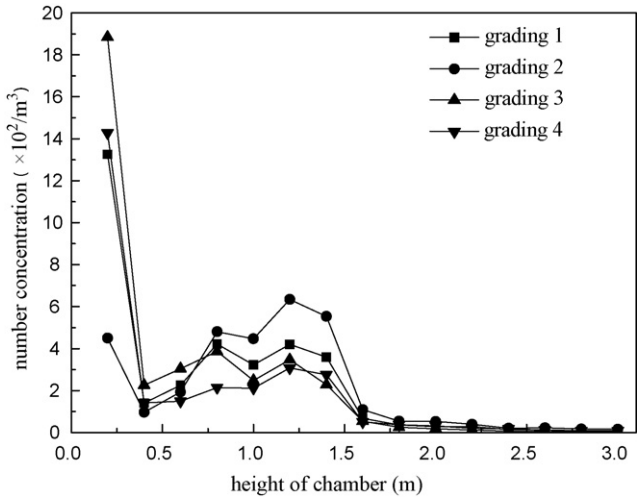

Fig. 14. The effects of particle size grading on axial distribution of particle number concentration.

Fig. 14 shows the axial distribution of particle number concentration with changing of particle size grading at an average gas inlet velocity of 3.0 m/s. The particle size grading listed in Table 2 is used in this simulation. At the bottom of the pool, the particle number concentration rises with the percentage of big particles increasing. Meanwhile, the number concentration of suspended particles in the pool increases with the percentage of small particles increasing. With changes of the particle size grading, the distribution of particles number concentration can be changed obviously in the pool of scrubbing-cooling chamber. For grading 4, most of the particles are with a diameter of 0.01 m and thus the particle number concentration reduces obviously.

5. Conclusions

A three-dimensional Euler–Lagrange model has been described in detail, which was established for the simulation on the motions of particles in scrubbing-cooling chamber of CWS entrained-flow gasifier. The axial distribution of particle number concentration and the gas-solid separation characteristics were investigated and the corresponding results were obtained.

Results show that the distribution of particle number concentration is wave-shaped in the pool of scrubbing-cooling chamber.

This phenomenon reflects the different motions of particles with different sizes. The obvious classification phenomenon of particle size exists in the pool of the scrubbing-cooling chamber, and particles with different diameters have different distributions. The big particles are easy to subside in the pool, and mostly distribute at the bottom of the pool. However, small particles mostly concentrate around the outlet of cooling tube and the liquid surface. The suspended particles in the region of liquid surface may be entrained with entrained liquid by the flowing gas. Therefore, the excellent structure of chamber influences on the effect of suspended particles sedimentation is necessary.

As a whole, the particle number concentration gradually decreases along the height of scrubbing-cooling chamber and the concentration of suspended or diffused particles increases with the enhancement of the gas flux. As the share of big particles increasing, the number concentration of subsided particles at the bottom of the pool increases. However, with the share of small particles increasing, the number concentration of suspended particles increases. In the pool of scrubbing-cooling chamber, the effects of particle size grading on the particles number concentration is obvious.

Simulation results indicate that the high particle capture efficiency can be achieved in the process of gas with particles passing through the pool. Under the calculation conditions of this study, the maximum value of particle capture efficiency is 98.1%. In a certain range, the particle capture efficiency increases with the increase of gas velocity. This study gives the first indications of particle distribution characteristics in scrubbing-cooling chamber, further optimum designs of the chamber are needed to develop to enhance the sedimentation of suspended particles.

Acknowledgements

This research is supported by Special Funds for Major State Basic Research Projects of China (2004CB217707). The authors wish to express their gratitude.

References

[1] X.L. Guo, Z.H. Dai, X. Gong, et al., Performance of an entrained-flow gasification technology of pulverized coal in pilot-scale plant, Fuel Process. Technol. 88 (2007) 451–459.
[2] H. Watanabe, M. Otaka, Numerical simulation of coal gasification in entrained flow coal gasifier, Fuel 85 (2006) 1935–1943.
[3] S. Kajitani, S. Hara, H. Matsuda, Gasification rate analysis of coal char with a pressurized drop tube furnace, Fuel 81 (2002) 539–546.
[4] H.J. Hurst, F. Novak, J.H. Patterson, Viscosity measurements and empirical predictions for some model gasifier slags, Fuel 78 (1999) 439–444.
[5] Y.Z. Zhao, Z.L. Gu, Y. Li, et al., Numerical simulation on turbulent flow and heat transfer of vertical pipe in quench chamber of coal gasifier, J. Chem. Ind. Eng. 54 (2003) 115–118.
[6] Y.F. Wang, R.H. Lu, Y.F. Su, et al., Temperature distribution in the scrubbing-cooling tube of the new type coal slurry gasifier, J. East China Univ. Sci. Technol. 32 (2000) 300–304.
[7] Y. Li, Z.L. Gu, Y.Z. Yu, et al., Heat and mass transfer inside a vertical pipe of quench chamber in coal gasifier, J. Chem. Eng. Chin. Univ. 14 (2000) 134–138.
[8] G.Q. Yang, B. Du, L.S. Fan, Bubble formation and dynamics in gas–liquid–solid fluidization—A review, Chem. Eng. Sci. 62 (2007) 2–27.
[9] Y. Li, J.P. Zhang, L.S. Fan, Numerical simulation of gas–liquid–solid fluidization systems using a combined CFD–VOF–DPM method: bubble wake behavior, Chem. Eng. Sci. 54 (1999) 5101–5107.
[10] G.D. Jin, Multi-scale modeling of gas–liquid–solid three-phase fluidized beds using the EMMS method, Chem. Eng. J. 117 (2006) 1–11.
[11] B.N. Murthy, R.S. Ghadge, J.B. Joshi, CFD simulation of gas–liquid–solid stirred reactor: prediction of critical impeller speed for solid suspension, Chem. Eng. Sci. 62 (2007) 7184–7195.
[12] X.Y. Zhang, G. Ahmadi, Eulerian–Lagrangian simulations of liquid–gas–solid flows in three-phase slurry reactors, Chem. Eng. Sci. 60 (2007) 5089–5104.
[13] B. Wang, A.B. Yu, Numerical study of the gas–liquid–solid flow in hydrocyclones with different configuration of vortex finder, Chem. Eng. J. 135 (2008) 33–42.
[14] J.U. Brackbill, B.D. Kothe, C. Zemach, A continuum method for modeling surface tension, J. Comput. Phys. 100 (1992) 335–354.
[15] V. Yakhot, S.A. Orzag, Renormalization group analysis of turbulence: basic theory, J. Sci. Comput. 12 (1986) 3–11.
[16] M.A. Habib, R.B. Mansour, H.M. Bsder, et al., Erosion and penetration rates of pipe protruded in a sudden contraction, Comput. Fluids 37 (2008) 146–160.
[17] Y. Tsuji, T. Tanaka, Cluster patterns in circulating fluidized beds predicted by numerical simulation (discrete particle model versus two-fluid model), Powder Technol. 95 (1998) 254–264.
[18] L.M. Zou, Y.C. Guo, C.K. Chan, Cluster-based drag coefficient model for simulating gas-solid flow in a fast-fluidized bed, Chem. Eng. Sci. 63 (2008) 1052–1061.
[19] J.P. Zhang, Y. Li, L.S. Fan, Discrete phase simulation of gas–liquid–solid fluidization systems: single bubble rising behavior, Powder Technol. 113 (2000) 310–326.
[20] J.P. Zhang, L.S. Fan, C. Zhu, et al., Dynamic behavior of collision of elastic spheres in viscous fluids, Powder Technol. 106 (1999) 98–109.
[21] B.Y. He, Study on multiphase flow characteristics of the new type of scrubbing-cooling chamber, Ph.D. Thesis, East China University of Science & Technology, 2005.
[22] P. Liovic, M. Rudman, J.L. Liow, Numerical modeling of free surface flows in metallurgical vessels, Appl. Math. Model. 26 (2002) 13–140.
[23] R.H. Lu, Study on gas–liquid flow characteristics in scrubbing-cooling chamber, Ph.D. Thesis, East China University of Science & Technology, 2005.